J. Fluid Mech. (1991), *vol.* 226, *pp.* 243–256
Printed in Great Britain

Thermal hydraulic jump: theory and experiment

By R. E. BADDOUR
Department of Civil Engineering, The University of Western Ontario, London, Ontario, Canada N6A 5B9

(Received 1 August 1990)

A thermally stratified internal hydraulic jump in a fresh water ambient, which has a temperature equal to or greater than 4 °C, is investigated theoretically and experimentally. The thermal jump solutions obtained using a nonlinear buoyancy function are compared with the density jump solutions obtained using a linear buoyancy function. The study reveals considerable difference between thermal and density jump behaviour in a range of temperature above 4 °C. The error of treating a thermal jump as a density jump is found to increase with Froude number and temperature difference and decrease with ambient temperature. Thermal jump experiments are conducted at ambient water temperatures of 4 °C and 16 °C. The two sets of experiments have identical Froude number, Reynolds number and temperature difference. Experimental observations compare favourably with the thermal jump theory. The analysis of temperature fluctuations suggests that ambient temperature is also modifying the internal mixing characteristics of thermal jumps.

1. Introduction

The *thermal hydraulic jump* is an internal jump which is thermally stratified. The density field in a thermal jump is therefore temperature dependent. On the other hand, the *density jump* terminology introduced by Wilkinson & Wood (1971) is adopted to refer to an internal jump when the density field is entirely dependent on the concentration of a dissolved substance (e.g. salt). Thermal and density jumps are similar but not identical. The difference in behaviour stems from the nature of the relationship between the buoyancy and the physical quantity that is causing it. In a density jump the buoyancy is a *linear* function of concentration, while in a thermal jump the buoyancy is a *nonlinear* function of temperature.

Since temperature differences in most water applications are relatively small (typically 10–15 °C), studies of thermal flows have systematically ignored the nonlinearity of the buoyancy–temperature relationship. This widespread assumption has not been scrutinized and, as will be shown, a linear approximation of the buoyancy function could lead to significant errors when miscible thermal flows are modelled numerically or physically as density flows. One of the objectives of this study is to examine theoretically and experimentally the behaviour of a thermal hydraulic jump. Another objective is to quantify the error caused by the linearization of the buoyancy function in the modelling of thermal jumps, or in other words the error of treating a 'thermal jump' as a 'density jump'.

The nonlinearity of the buoyancy function is quite pronounced when the ambient water temperature approaches 4 °C, i.e. the temperature of maximum density. Furthermore, the buoyancy of a thermal flow may change direction when the

temperature of ambient drops below 4 °C. This buoyancy reversal, which occurs in cold climate regions, is not addressed in this paper, and only situations with ambient temperature equal or greater than 4 °C are discussed.

2. Equation of state

We consider first the equation of state of fresh water $\rho = \rho(T)$, where ρ is the density in kg/m^3 and T the temperature in degrees Celcius. The density is of the order of 1000 kg/m^3 and the maximum variation in density for $0 < T < 35$ °C is only 6 kg/m^3. To avoid such small differences in large numbers, the equation of state can be normalized and expressed as $\rho' = \rho'(T')$, where $\rho' = (\rho_m - \rho)/(\rho_m - \rho_r)$ and $T' = T/T_r$. The maximum density at $T = 4$ °C is $\rho_m = 1000$ kg/m^3, and the reference temperature is $T_r = 35$ °C. The water equation of state normalized in this manner is plotted in figure 1 and accurately fitted with the polynomial

$$\rho' = \sum_{i=0}^{n} a_i T'^i. \tag{1}$$

A fifth-degree polynomial was implemented in this study. The accuracy of density calculations with this polynomial is on average 0.08% in the range of temperature $0 < T < 35$ °C.

3. The buoyancy function

The buoyancy force acting on a unit volume is $\Delta\rho\, g$, where $\Delta\rho = (\rho_a - \rho)$ is the density difference with respect to ambient density ρ_a, and g is the gravity constant. A buoyancy function of excess temperature $\theta = (T - T_a)$ with respect to ambient temperature T_a is obtained from (1). The transformation is

$$g' = g\left(\frac{\Delta\rho}{\rho_a}\right) = g\left(\frac{\rho_m - \rho_r}{\rho_a}\right)\sum_{i=1}^{n} b_i \theta'^i \tag{2}$$

where the coefficients b_i; $i = 1, n$ are determined from the expression

$$b_i = \sum_{j=i}^{n} \frac{j(j-1)(j-2)\ldots(j-i+1)}{i!} a_j T_a'^{j-i}; \quad i = 1, n \tag{3}$$

and $\theta' = (T - T_a)/T_r$ and $T'_a = T_a/T_r$. The buoyancy force per unit mass g', in a stratified flow, is analogous to the gravity force per unit mass g in a single-layer free-surface flow.

4. Governing equations

We now consider a thermal hydraulic jump generated by a turbulent supercritical discharge of warm water at the surface of a colder water body in a deep channel. (Extending the definitions from single-layer open channel hydraulics, the flow of thickness y is supercritical when the velocity v exceeds the velocity of propagation of the fastest infinitesimal long internal wave, i.e. $v > (g'y)^{\frac{1}{2}}$, and hence the Froude number $v/(g'y)^{\frac{1}{2}} > 1$. Similarly, the flow is subcritical when the Froude number is less than 1.) The temperature T_a of the receiving water is constant and greater than 4 °C. The flow is depicted in figure 2. The volume flux of warm water entering the

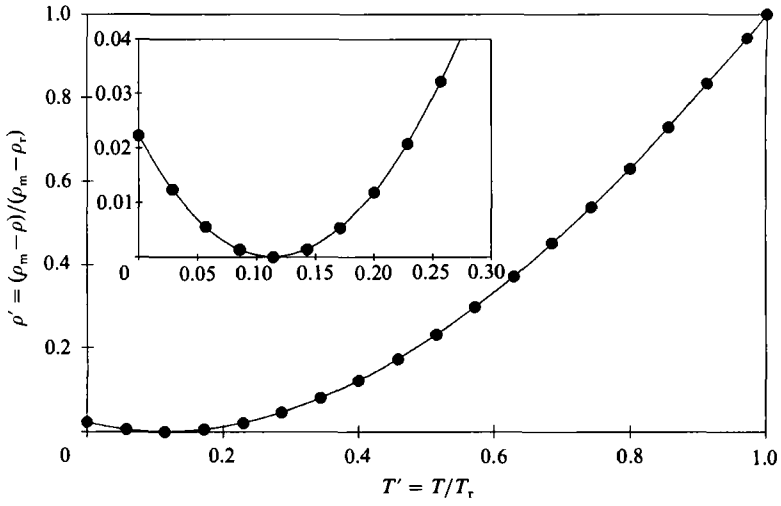

FIGURE 1. Normalized equation of state; $T_m = 4$ °C, $T_r = 35$ °C, $\rho_m = 1000$ kg/m^3, $\rho_r = 994.0635$ kg/m^3; ●, water data; ——, fifth degree polynomial, $a_0 = 0.022302$, $a_1 = -0.40026$, $a_2 = 1.874472$, $a_3 = -0.73126$, $a_4 = 0.306327$, $a_5 = -0.07157$.

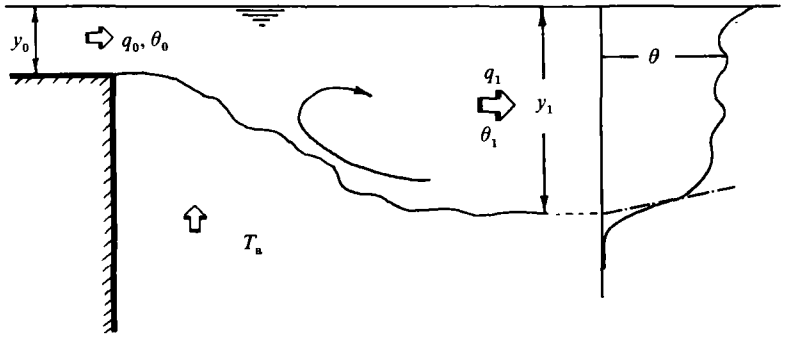

FIGURE 2. Definition sketch of a thermal hydraulic jump.

channel per unit width is q_0. Also defining the source condition are the excess temperature θ_0 of the discharge above ambient temperature T_a and the initial depth of the discharge y_0. Within a relatively short distance, the flow undergoes a rapid transition and a stable subcritical flow is established. In this type of flow, when the discharge and ambient fluids are miscible the jump solution is not unique and the subcritical state depends as well on a hydraulic control which must exist in a channel further downstream. The reader is referred to Wilkinson & Wood (1971) and Baddour (1987) for more details on the hydraulics of this flow in deep and shallow channels. Since ambient water may be entrained and mixed with the surface discharge, the volume flux of warm water downstream of the jump is $q_1 > q_0$, the corresponding excess temperature is $\theta_1 < \theta_0$ and the depth is y_1. In this study the mean temperature profiles measured downstream of the jump were generally found to approach a uniform shape (see figure 12) with a deviation from uniform near the surface and a steep gradient at the interface. In the following, both temperature and velocity are assumed uniformly distributed downstream of the jump.

For a steady flow and within the Boussinesq approximation ($\Delta\rho/\rho \ll 1$) the two equations governing the behaviour of the thermal jump are

$$q_0\theta_0 = q_1\theta_1 \tag{4}$$

and
$$\tfrac{1}{2}g_0' y_0^2 + \frac{q_0^2}{y_0} = \tfrac{1}{2}g_1' y_1^2 + \frac{q_1^2}{y_1}, \tag{5}$$

where $g_0' = g(\rho_a - \rho_0)/\rho_a$ and $g_1' = g(\rho_a - \rho_1)/\rho_a$. Equation (4) conserves the excess temperature flux and (5) conserves the momentum function (i.e. the sum of the momentum flux and excess hydrostatic force). These two equations extend the well-known formulation of a hydraulic jump in a single-layer open channel flow which may be traced back to the work of Belanger† (1850).

In a non-dimensional form, (5) is

$$\tfrac{1}{2} + F_0^2 = \tfrac{1}{2}r_1^2\left(\frac{g_1'}{g_0'}\right) + F_0^2\left(\frac{S_1^2}{r_1}\right), \tag{6}$$

where the dilution $S_1 = q_1/q_0$, the conjugate depth ratio $r_1 = y_1/y_0$, and the Froude number $F_0 = (q_0/y_0)/(g_0' y_0)^{\frac{1}{2}}$. In the case of an immiscible flow [i.e. $S_1 = 1$ and $g_1'/g_0' = 1$], (6) has the unique physical solution

$$r_1 = r_1^* = \tfrac{1}{2}[(1 + 8F_0^2)^{\frac{1}{2}} - 1]. \tag{7}$$

Equation (7) is identical to the classical hydraulic jump equation for single-layer open channel flow with the Froude number representing the ratio of inertia and buoyancy forces rather than inertia and gravity forces, respectively. The similarity of internal and free-surface jumps was recognized in previous studies by Long (1953), Benton (1954) and Yih & Guha (1955).

For a miscible thermal flow, however, the buoyancy ratio (g_1'/g_0') in (6) must be determined from (2) and (4). Accordingly the equation governing the thermal jump is

$$\tfrac{1}{2} + F_0^2 = \tfrac{1}{2}r_1^2 \frac{\sum_{i=1}^{n} \frac{b_i \theta_0'^i}{S_1^i}}{\sum_{i=1}^{n} b_i \theta_0'^i} + F_0^2 \frac{S_1^2}{r_1}. \tag{8}$$

When the buoyancy function is approximated with a straight line, only the first coefficient b_1 is retained in the two summations appearing on the right-hand side of (8). This linear approximation gives

$$\tfrac{1}{2} + F_0^2 = \frac{1}{2}\frac{r_1^2}{S_1} + F_0^2 \frac{S_1^2}{r_1}, \tag{9}$$

which is the equation governing the miscible behaviour of a density jump, and is consistent with the results of Wilkinson & Wood (1971).

The possible error resulting from the linearization of the buoyancy function in the modelling of thermal jumps will be examined in the following. Thermal and density

† Jean Baptiste Belanger (1850, pp. 132–146) considered the hydraulic jump and reviewed earlier work on this flow by George Bidone (1820). Bidone, who conducted an experimental study, is to be credited for introducing the now familiar terms 'remous' (i.e. roller) and 'ressaut' (i.e. jump) in the description of this flow. In his analysis, however, Bidone initially visualized the jump as a jet impinging on a moving plate, without loss of energy resulting from the impact. To obtain a reasonable agreement with the experimental data, Bidone subsequently proposed in his study an arbitrary correction factor to the velocity head. On the other hand, Belanger who recognized the rapidly varied character of the flow, ignored wall friction and applied Newton's momentum/impulse principle to the jump. Using the momentum rather than the energy principle, Belanger (1850, pp. 138) obtained an expression for the depth downstream of the jump as a function of depth and velocity upstream. The equation derived by Belanger is correct and equivalent to equation (7).

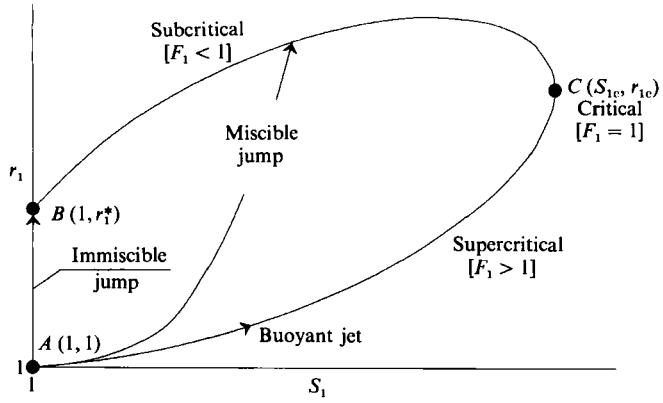

FIGURE 3. Internal hydraulic jump solutions.

jumps solutions obtained using (8) and (9) will also be compared with experimental observations.

5. Jump solutions

In the thermal jump experiment the dilution S_1 was controlled, and is treated, therefore, as an independent variable. When S_1 is specified in (8) or (9) it is possible to determine the conjugate depth ratio r_1 by solving a cubic equation. The physical domain of the solution was found in the (S_1, r_1)-plane to be bounded by a maximum dilution S_{1c} and a maximum depth ratio r_{1m}. The constraints defining the physical domain of the jump solution are: (i) $r_1 \geqslant 0$, (ii) $S_1 \geqslant 1$ and (iii) $[y_0 + v_0^2/2g_0'] \geqslant [y_1 + v_1^2/2g_1']$. Constraint (iii) allows a loss of energy in the direction of flow, and, as in the case of a free-surface flow, eliminates the physical possibility of a jump from a subcritical to a supercritical regime. The solution consists of two limbs AC and BC joined at C as illustrated in figure 3. The lower limb AC is supercritical (i.e. $F_1^2 = q_1^2/(g_1' y_1^3) > 1$) and connects the initial supercritical state $A(1, 1)$ to the critical state $C(S_{1c}, r_{1c})$ where $F_1^2 = 1$. The upper limb BC is, on the other hand, subcritical (i.e. $F_1^2 < 1$) and connects the immiscible jump state $B(1, r_1^*)$ to C. The immiscible jump solution $r_1 = r_1^*$ defining point B on the r_1 axis of figure 3 was given in (7).

Thermal and density jump solutions are compared in figure 4 for a discharge Froude number $F_0 = 50$ and an initial temperature difference $\theta_0 = 10$ and 15 °C. These plots clearly show the profound effect the nonlinearity of the buoyancy function may have on the jump solutions.

It can be noted, however, in figure 4 that the thermal solution converges to the density solution when the ambient temperature is sufficiently high ($T_a' > 30$ °C). Furthermore, the difference in behaviour between a thermal and a density jump appears quite significant in a range of temperature above 4 °C. As expected the difference in behaviour increases as the ambient temperature decreases and approaches 4 °C.

For a density jump the maximum dilution S_{1c} and the critical depth r_{1c} may be determined from (9) by setting $\mathrm{d}S_1/\mathrm{d}r_1 = 0$. They are respectively given by

$$S_{1c} = \tfrac{1}{3} F_0^{-\frac{4}{3}}(1 + 2F_0^2) \tag{10}$$

and

$$r_{1c} = \tfrac{1}{3} F_0^{-\frac{2}{3}}(1 + 2F_0^2). \tag{11}$$

A similar critical state exists in the case of a thermal jump in a deep ambient, but it must be determined numerically. The critical state defined by S_{1c} and r_{1c} can be

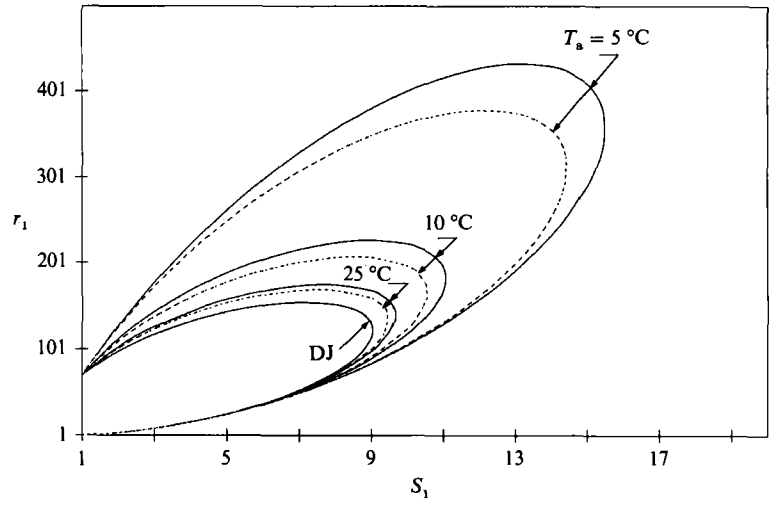

FIGURE 4. Comparison of thermal and density jump solutions; $F_0 = 50$; ——, $\theta_0 = 15$ °C; - - -, $\theta_0 = 10$ °C; DJ = density jump.

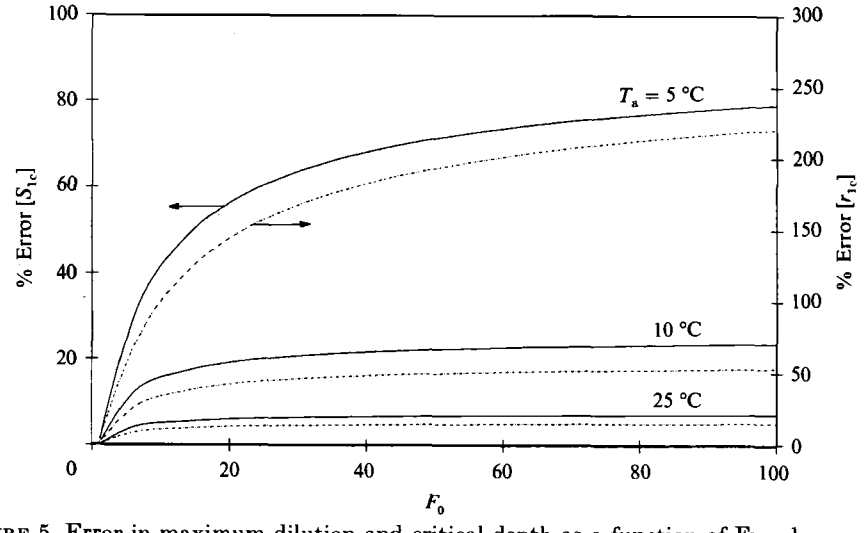

FIGURE 5. Error in maximum dilution and critical depth as a function of Froude number; $\theta_0 = 15$ °C; ——, S_{1c}; - - -, r_{1c}.

used to quantify the magnitude of the error caused by the linearization of the buoyancy function. Figure 5, for example, shows the effect of Froude number on the error in calculations of maximum dilution and depth when the buoyancy function is linearized. The error initially increases with Froude number and approaches a maximum value at large Froude numbers.

6. Thermal jump experiment

The thermal jump experiment was conducted in a channel 2.5 m long, 0.15 m wide and 0.5 m high, figure 6. The testing section was 1.35 m long and 0.35 m deep. The channel was constructed with double acrylic walls and an air gap in between. This design minimized heat exchange with the surroundings and eliminated the

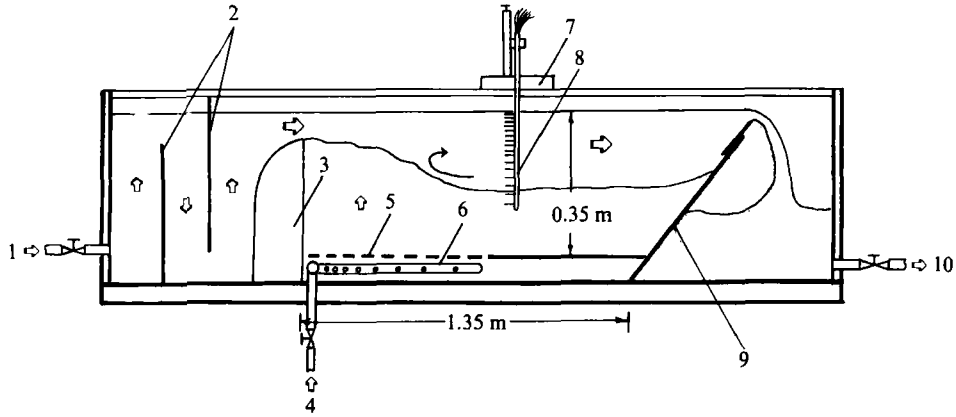

FIGURE 6. Experimental apparatus: 1, warm water supply; 2, baffles; 3, round-crested weir; 4, cold water supply; 5, perforated plate; 6, diffusers; 7, carriage; 8, probes; 9, inclined gate; 10, drain.

Test	T_0 (°C)	T_a (°C)	q_0 (cm²/s)	y_0 (cm)	S_1 (q_1/q_0)	y_1 (cm)
S4	31.0	16.0	8.7	0.95	2.0	7.5
W4	19.0	4.0	12.5	1.60	2.0	16.0
SF4	31.0	16.0	8.7	0.95	1.5	7.4
WF4	19.0	4.0	12.5	1.60	1.5	14.2

TABLE 1. Summary of test conditions; $F_0 = 5$; $Re_0 = 4000$

condensation problem when the ambient water in the channel was colder than room temperature. A cooling system controlled the temperature of the ambient water, and a mixing valve the temperature of the discharge. The supplies of warm and cold water to the apparatus were monitored with flowmeters and adjusted with valves. The warm water entered the testing section over a smooth and round-crested weir. Baffle plates installed in the inlet compartment of the channel helped to remove air bubbles present in the warm water discharge. The depth of the discharge at the entrance of the testing section was adjusted by raising or lowering an inclined tail gate. During the experiment, cold water was continuously introduced into the channel via two bottom line diffusers. The diffusers had a series of horizontal ports pointing to each other. The ports were designed to provide a diminishing rate of ambient supply with distance away from the entrance. The diffusers were also capped with a horizontal perforated plate.

The temperature was measured in this experiment with an array of 15 thermocouple probes. The diameter of the thermocouple wires was 0.12 mm and the response time of these probes was 0.01 s. The temperature data were gathered with a data acquisition system (Keithly series 500) in conjunction with an IBM PC. A thermocouple module (AIM7) and a 12-bit analog-to-digital module (ADM1) allowed temperature to be measured with an accuracy of 0.1 °C. The system was programmed to scan the output from the 15 probes simultaneously at a frequency of 10 Hz per probe for a period of 100 s. The test conditions of the thermal jump experiment are summarized in table 1.

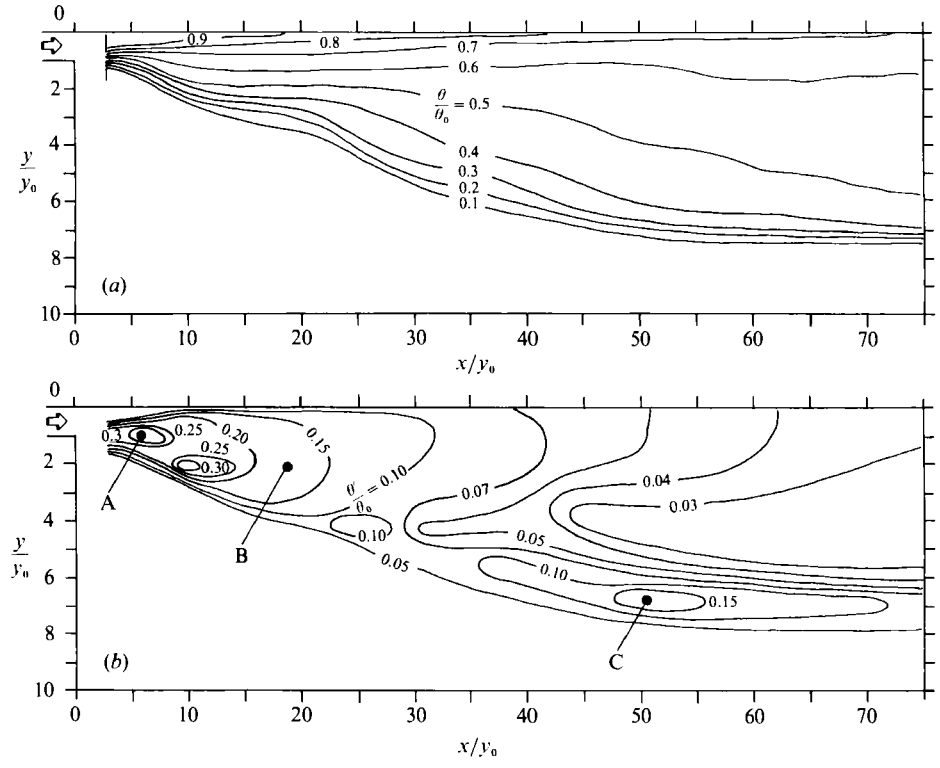

FIGURE 7. Thermal jump results: test S4. (*a*) Contours of mean excess temperature θ/θ_0; (*b*) contours of r.m.s. temperature fluctuation θ'/θ_0.

7. Experimental results

The mean and r.m.s. temperature fields for tests S4 and W4 are presented in figures 7 and 8. The iso-mean and iso-intensity contours were obtained from a grid of about 15 × 15 data points. Tests S4 and W4 were designed to have the same Froude number $F_0 = 5$, Reynolds number $Re_0 = 4000$, dilution $S_1 = 2$, and initial excess temperature $\theta_0 = 15$ °C. The remarkable difference in the results of these two tests is, therefore, attributed to the non-linearity of the buoyancy function. Note, the ambient temperature of test S4 is 16 °C, and the ambient temperature of test W4 is only 4 °C.

To examine the effect of ambient temperature on the internal mixing characteristics, the temperature fluctuations at three strategic locations in jumps S4 and W4 are compared in the following. S4 and W4 will be referred to as *summer* and *winter* tests, since they respectively simulate summer and winter conditions of a thermal discharge into a fresh water environment. The three locations chosen for this comparison are denoted in figures 7 and 8 as A, B and C. Location A is in the centre of the mixing layer, within a short distance from the discharge, location B is in the centre of the shear layer just upstream of the roller, and location C is in the interfacial region of the subcritical flow, downstream of the jump. Figures 9–11 show the temperature traces, and power density spectra obtained at A, B and C. The spectra were calculated using a fast Fourier transformation algorithm (IMSL Fortran Library).

In the early stage of development the summer flow appears to be more stable than the winter flow and the large turbulent structures are more organized. A single

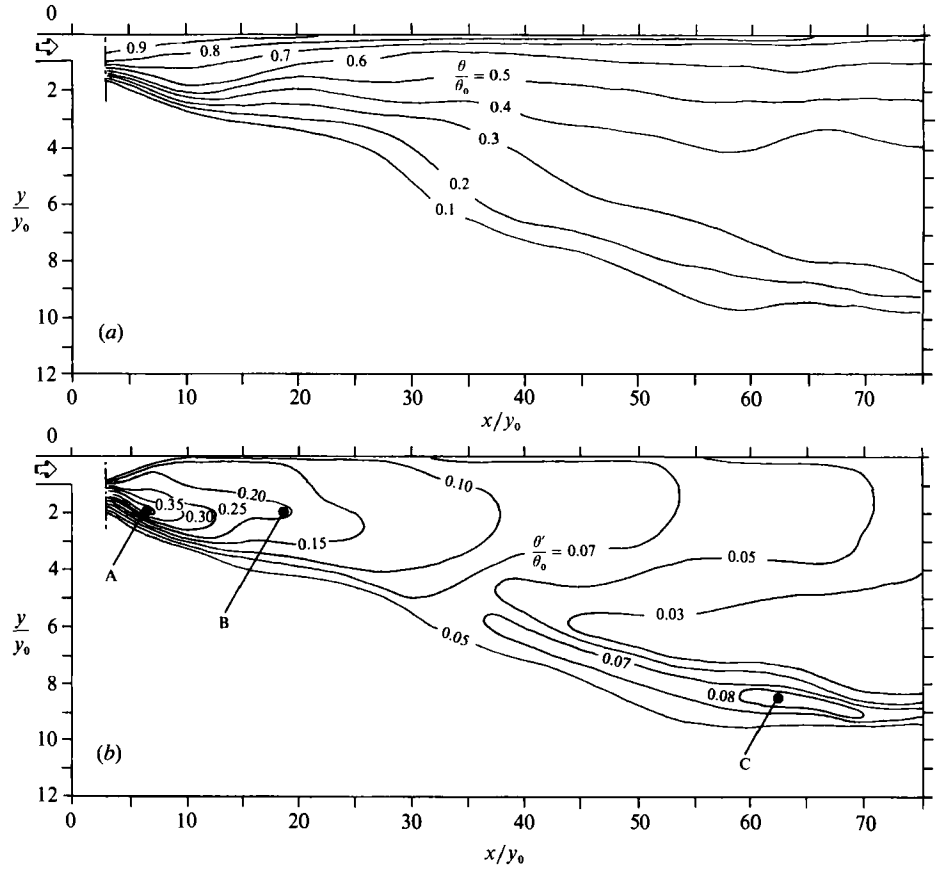

FIGURE 8. Thermal jump results: test W4. (*a*) Contours of mean excess temperature θ/θ_0; (*b*) contours of r.m.s. temperature fluctuation θ'/θ_0.

dominant frequency of about 2 Hz may be noted in the spectrum of trace A of test S4. On the other hand, three dominant frequencies smaller than 1 Hz appeared in the spectrum of trace A of test W4, suggesting a higher degree of instability. Also at A the probability distribution of temperature is skewed towards the discharge temperature in test S4, and towards the ambient temperature in test W4. At B the probability distribution of temperature fluctuation is essentially Gaussian in the summer flow and has a double peak structure in the winter flow. These observations suggest that summer and winter flow have different internal mixing characteristics. At identical Froude number and Reynolds number, the turbulence in the winter flow appears less capable of internally mixing the flow than the summer flow. This behaviour is related to a lack of small-scale eddies as seen in the spectra. The poor internal mixing in the winter flow explains why the temperature fluctuations are consistently higher upstream of the roller of test W4 than in test S4 (see figures 7*b* and 8*b*). Finally, the temperature fluctuations at location C are the reflection of internal wave motions at the interface of the subcritical flow downstream of the jump. The summer flow has a sharper interface and higher frequency of temperature fluctuations. The nonlinearity of the buoyancy function creates in the winter flow small density gradients and hence produces an unstable and more diffused interface.

Typical instantaneous temperature profiles obtained downstream of the jump are shown in figure 12. The instantaneous maximum gradient of temperature provided

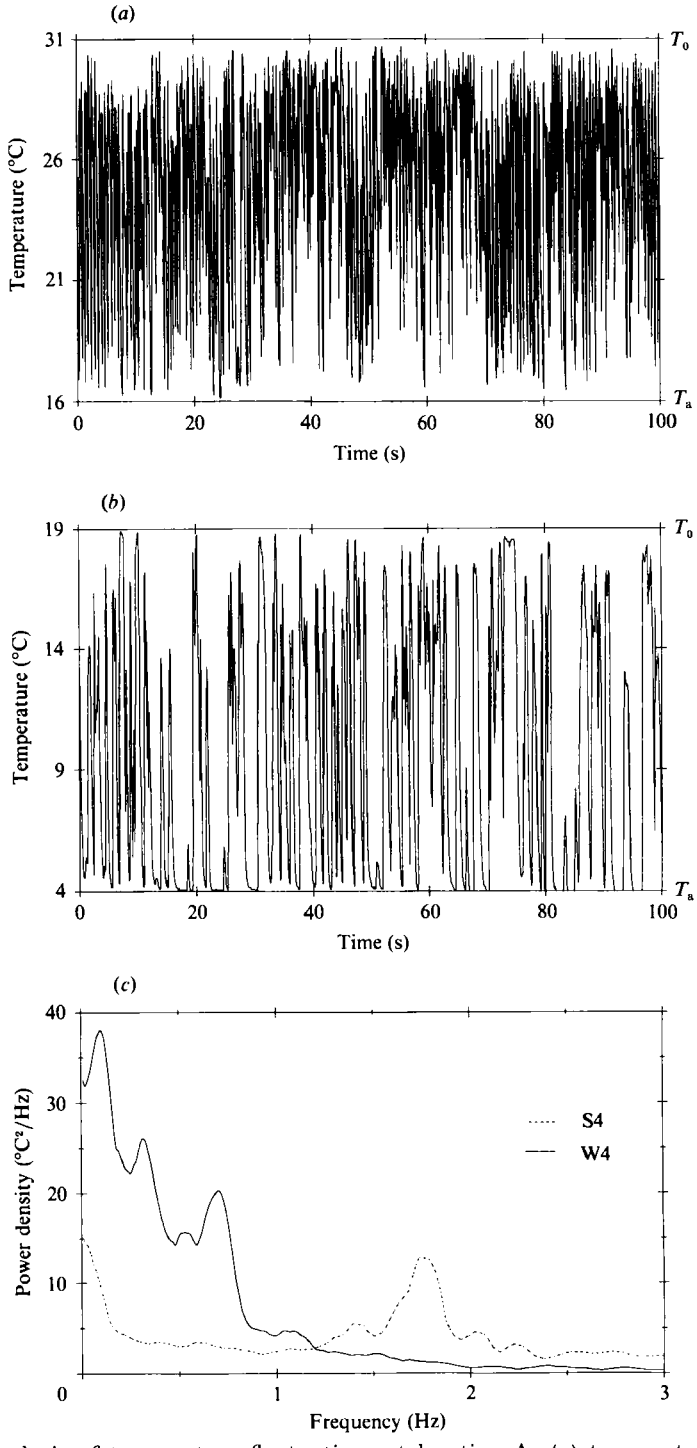

FIGURE 9. Analysis of temperature fluctuations at location A: (*a*) temperature trace, test S4; (*b*) temperature trace, test W4; (*c*) power density spectra.

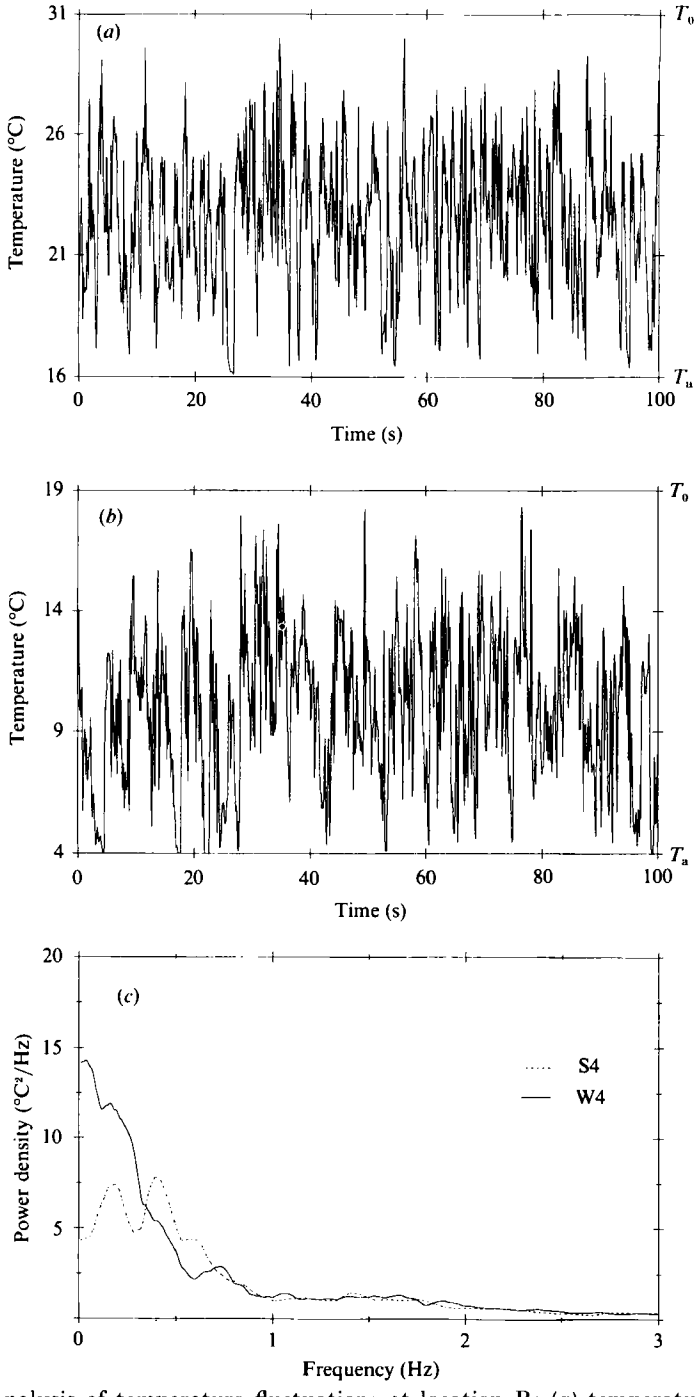

FIGURE 10. Analysis of temperature fluctuations at location B: (*a*) temperature trace, test S4; (*b*) temperature trace, test W4; (*c*) power density spectra.

a suitable means of defining the position of the interface at any given time. This was accomplished by fitting the data in the interface region with a polynomial. The coefficients of the polynomial were then used to calculate the maximum gradient, and accordingly the instantaneous location of the interface. This procedure generated

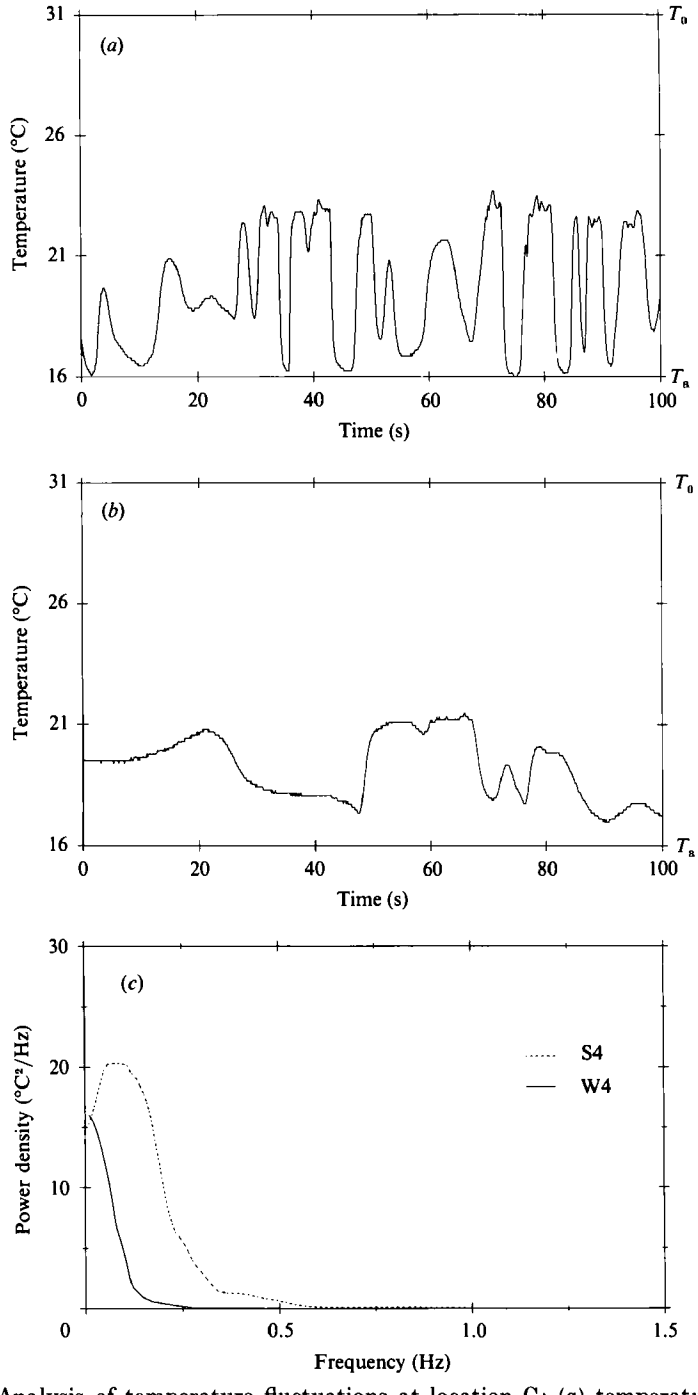

FIGURE 11. Analysis of temperature fluctuations at location C: (*a*) temperature trace, test S4; (*b*) temperature trace, test W4; (*c*) power density spectra.

time traces of the depth of the surface layer and revealed the characteristics of the internal wave motion at the interface.

Figure 13 shows the time history of the interface for tests S4 and W4. It may be noted that the interface was essentially at a constant depth, most of the time.

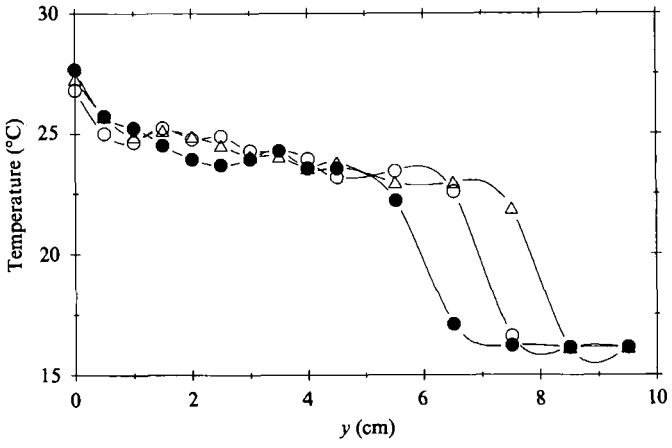

FIGURE 12. Instantaneous temperature profiles downstream of the jump, test S4, $x = 65$ cm; ○, $t = 19.6$ s; ●, $t = 38.7$ s; △, $t = 63.7$ s.

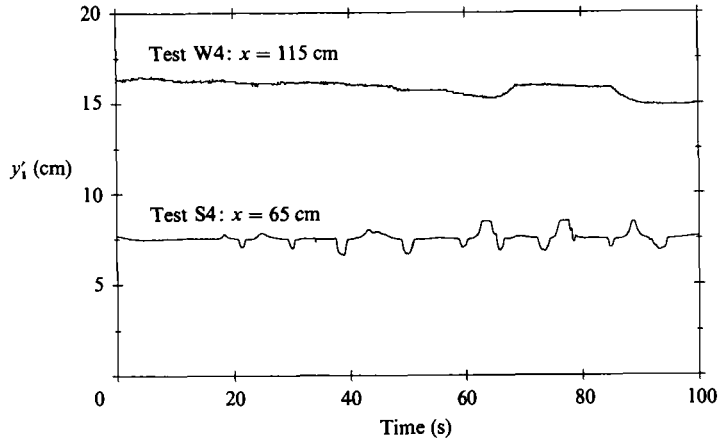

FIGURE 13. Time history of interface depth downstream of the jump.

Nevertheless, it was disturbed by internal waves travelling back and forth within the limited space of the testing section. Time series of the interface depth were used to calculate the most probable thickness of the layer downstream of the jump.

A comparison of the thermal jump theory with the experiment is presented in figure 14. The conjugate depth y_1 was determined for each test using the time series of the interface depth in the subcritical region. The depth corresponding to the peak of the probability distribution was assumed to represent y_1. The values of y_1 obtained in this manner are given in table 1. Mean and median estimates provided essentially the same results. With the exception of test W4, the experimental data in figure 14 are in good agreement with the thermal jump theory. The depth y_1 for Test W4 is less than predicted by the theory, but this case represents the deepest and longest jump examined in this study. The depth y_1 was 0.16 m and was measured at a distance of 1.15 m from the discharge. Since the testing section was only 1.35 m long and 0.35 m deep, it is possible that the development of this jump was affected by the limited size of the testing section.

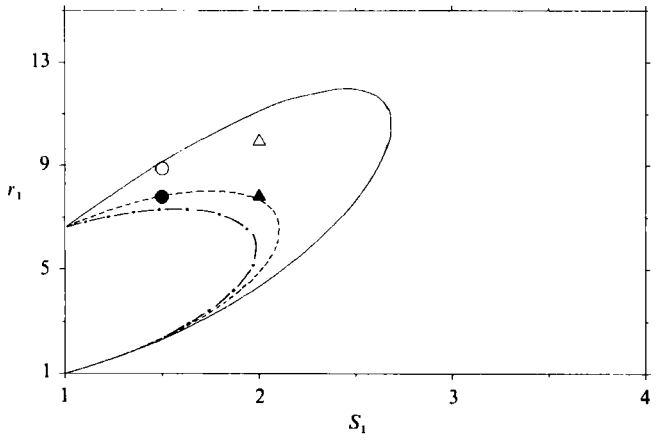

FIGURE 14. Comparison of thermal jump theory with experiment: $F_0 = 5$; $\theta_0 = 15$ °C. Experiment: ●, SF4; ○, WF4; ▲, S4; △, W4. Theory: —·—, DJ; ----, $T_a = 16$ °C; —, $T_a = 4$ °C.

8. Concluding remarks

In addition to the Froude number, consideration must be given to both the ambient temperature and the temperature difference when modelling thermal jumps. These two additional parameters are connected to the nonlinearity of the buoyancy function. This study examined the effect of these parameters on the behaviour of a thermal jump and quantified the error expected when these parameters are ignored. The effects associated with the non-linearity of the buoyancy function were found to be relevant when the ambient temperature was less than about 15 °C. Summer and winter experiments with identical Froude number and Reynolds number had markedly different structures of temperature fluctuations, and the summer flow showed better internal mixing capabilities than the winter flow.

Mr L.-L. Guo assisted in conducting the thermal jump experiment. The financial support was provided by the Natural Sciences and Engineering Research Council of Canada.

REFERENCES

BADDOUR, R. E. 1987 Hydraulics of shallow and stratified mixing channel. *J. Hydraul Engng Div. ASCE* **113**, 630–645.

BELANGER, J. B. 1850 Notes sur le cours d'hydraulique. *Ecole Centrale des Arts et Manufactures*, France.

BENTON, G. S. 1954 The occurrence of critical flow and hydraulic jumps in a multi-layered fluid system. *J. Met.* **11**, 139–150.

BIDONE, G. 1820 Expérience sur le remous et la propagation des ondes. *Mém. Acad. Sci. Turin* **25**, 21–112.

LONG, R. R. 1953 Some aspects of the flow of stratified fluids: a theoretical investigation. *Tellus* **5**, 42–58.

WILKINSON, D. L. & WOOD, I. R. 1971 A rapidly varied flow phenomenon in a two-layer flow. *J. Fluid Mech.* **47**, 241–256.

YIH, C.-S. & GUHA, C. R. 1955 Hydraulic jump in a fluid system of two layers. *Tellus* **7**, 358–366.